A nontransferring dry adhesive with hierarchical polymer nanohairs

Hoon Eui Jeong[a,1], Jin-Kwan Lee[b,1], Hong Nam Kim[a], Sang Heup Moon[b,2], and Kahp Y. Suh[a,c,2]

[a]School of Mechanical and Aerospace Engineering, [b]School of Chemical and Biological Engineering, and [c]Institute of Advanced Machinery and Design, Seoul National University, Seoul 151-742, Korea

Edited by Robert Langer, Massachusetts Institute of Technology, Cambridge, MA, and approved February 13, 2009 (received for review January 13, 2009)

We present a simple yet robust method for fabricating angled, hierarchically patterned high-aspect-ratio polymer nanohairs to generate directionally sensitive dry adhesives. The slanted polymeric nanostructures were molded from an etched polySi substrate containing slanted nanoholes. An angled etching technique was developed to fabricate slanted nanoholes with flat tips by inserting an etch-stop layer of silicon dioxide. This unique etching method was equipped with a Faraday cage system to control the ion-incident angles in the conventional plasma etching system. The polymeric nanohairs were fabricated with tailored leaning angles, sizes, tip shapes, and hierarchical structures. As a result of controlled leaning angle and bulged flat top of the nanohairs, the replicated, slanted nanohairs showed excellent directional adhesion, exhibiting strong shear attachment (≈26 N/cm^2 in maximum) in the angled direction and easy detachment (≈2.2 N/cm^2) in the opposite direction, with a hysteresis value of ≈10. In addition to single scale nanohairs, monolithic, micro-nanoscale combined hierarchical hairs were also fabricated by using a 2-step UV-assisted molding technique. These hierarchical nanoscale patterns maintained their adhesive force even on a rough surface (roughness <20 μm) because of an increase in the contact area by the enhanced height of hierarchy, whereas simple nanohairs lost their adhesion strength. To demonstrate the potential applications of the adhesive patch, the dry adhesive was used to transport a large-area glass (47.5 × 37.5 cm^2, second-generation TFT-LCD glass), which could replace the current electrostatic transport/holding system with further optimization.

biomimetics | gecko | angled etching | slanted nanohair | hierarchical nanohair

Adhesive are used in many aspects of the daily life. With increasing demands for various applications in the industry, new adhesives have been developed that use thermoplastic, UV or light curing, rubbery and pressure-sensitive materials (1). In general, such man-made adhesives have high (sometimes extremely strong) adhesion strength but are not easily detached. Furthermore, they are seldom reusable because the surfaces are quickly contaminated by adhering materials because of their tacky nature. In contrast, nature has created its own adhesives with unique structures and functions. For example, mussels generate specialized adhesive proteins, allowing for strong adhesion to wet surfaces, which is not easily achievable with man-made adhesives (2).

In addition, dry adhesion mechanism in gecko lizards has attracted much attention because it provides strong, yet reversible attachment against surfaces of varying roughness and orientation. Such unusual adhesion capability is attributed to arrays of millions of fine microscopic foot hairs (setae), splitting into hundreds of smaller, nanoscale ends (spatulae), which form intimate contact to various surfaces by van der Waals forces with strong adhesion (≈10 N/cm^2) (3, 4). Recently, extensive studies have been made to mimic gecko foot hairs toward a new nature-inspired artificial dry adhesive. Several groups have demonstrated that structural features (e.g., size, aspect ratio, tilted angle, tip shape, and hierarchy) should be carefully optimized for an artificial dry adhesive with high performance (5–8). For example, fabrication of slanted, high-aspect-ratio (AR) nanostructures is essential for synthetic dry adhesives because structures with higher AR enhance the adhesive force due to higher elastic energy dissipation at pull-off, increased number of pillars at the time of contact, and decrease of effective modulus (5, 9, 10). According to the contact splitting theory, decrease of pillar diameter also significantly enhances the adhesion (5, 11). In addition to high AR and small radius of structures, a directional angle of nanostructure is an another crucial factor for anisotropic, reversible dry adhesive because an angled structure significantly lowers the effective modulus of the surface (10). More importantly, anisotropic adhesion property (i.e., strong attachment and easy detachment) could be obtained with slanted structures of a directional angle because such a surface is only adhesive when loaded in a particular direction (12, 13). Thus, the fabrication of angled, high-AR nanostructures is of great benefit for the development of an artificial dry-adhesive. In addition to these requirements, a hierarchy of multiscale structures may better mimic gecko foot hairs with enhanced structural compliance and adaptability against various rough surfaces (14–16).

To date, a number of methods have been introduced to fabricate vertical, high-AR nanostructures, which include e-beam lithography (17), nanomolding (8), stretching of a polymer film (18), replicating a nanoporous membrane with polymer (19), and growth of carbon nanotubes (20, 21). Although these approaches are useful, angled structures cannot be easily acquired with these methods. Moreover, they need an expensive and sophisticated process, limiting widespread uses of the methods. For fabricating angled structures, a modified photolithographic method combined with soft lithography has been proposed (9, 13, 22). A range of angled microstructures were successfully fabricated with these methods, demonstrating that the angled structures are essential for directional adhesion (13). These methods, however, have potential limitations such as low resolution, low AR, and lack of geometrical controllability, resulting in reduced adhesive force and directionality. In addition, a structural hierarchy cannot be easily achieved with the aforementioned techniques.

Here, we present a simple, yet robust technique of fabricating high-AR, inclined polymer nanostructures with controllable geometry (angle, diameter, height, tip shape, and hierarchy) by employing replica molding with an UV-curable polymer and angled etching of polySi substrate. As described below, a thin dry adhesive with angled nanohairs shows excellent directional adhesion as well as high shear adhesion strength (≈26 N/cm^2 in maximum) that are enabled by intrinsic characteristics of the slanted, high-AR polymer nanohairs. In addition to single-scale nanohairs, micro-/nanoscale

Author contributions: H.E.J., J.-K.L., S.H.M., and K.Y.S. designed research; H.E.J., J.-K.L., and H.N.K. performed research; H.E.J. and J.-K.L. analyzed data; and H.E.J., J.-K.L., S.H.M., and K.Y.S. wrote the paper.

The authors declare no conflict of interest.

This article is a PNAS Direct Submission.

[1]H.E.J. and J.-K.L. contributed equally to this work.

[2]To whom correspondence may be addressed. E-mail: shmoon@surf.snu.ac.kr or sky4u@snu.ac.kr.

This article contains supporting information online at www.pnas.org/cgi/content/full/0900323106/DCSupplemental.

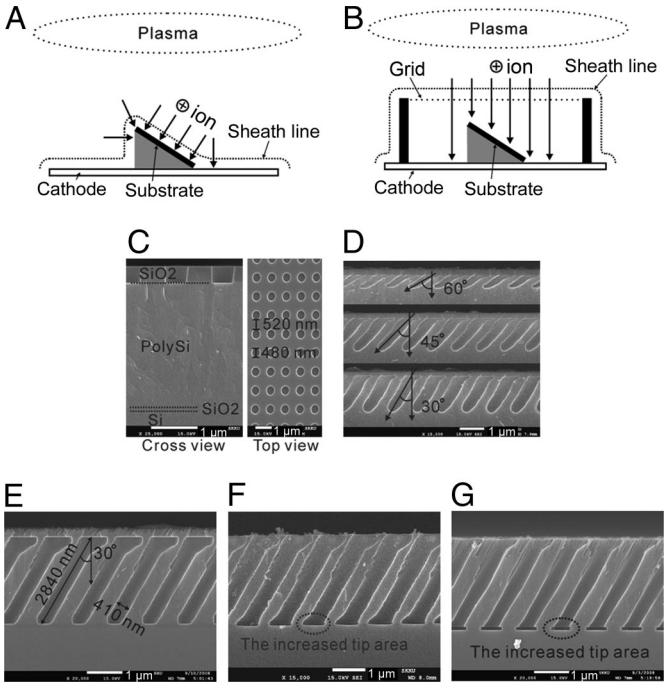

Fig. 1. Mechanism and fabrication results of angled etching technique. (*A*) An illustration of the plasma sheath without a Faraday cage. Ions are incident on the substrate surface in a direction normal to the substrate surface. (*B*) An illustration of the plasma sheath with a Faraday cage. Ions are incident on the substrate surface in a direction normal to the grid plane. (*C*) SEM images of polySi substrates used in the etching experiment. (*D*) SEM images of polySi etch profiles with angles of 30°, 45°, and 60°. The images indicate that the angle of etch profiles can be controlled by using the Faraday cage system. (*E–G*) SEM images of polySi masters for the fabrication of nanohairy structures. Etch profiles have an angle of 30° and an aspect ratio of 6.9 (etch depth = 2,840 nm; the hold CD = 410 nm), as shown in *E*. By using the etch-stop layer, the flat bottom surface was obtained. The surface area of the bottom could be further increased by an over-etching of the polySi (*F*) and a wet etching of the etch-stop layer (*G*).

combined hierarchical structures with high AR and directional angle were also fabricated by using a 2-step UV-assisted capillary molding technique. These hierarchical multiscale hairs exhibit high adhesive capability even on a rough surface (roughness <20 μm) compared with simple nanohairs. Furthermore, the potential application of such adhesives is demonstrated by applying the dry adhesive to transport a large glass tile.

Results and Discussion

Angled Etching Technique. Fabrication of angled nanoholes with a high AR has been elusive because of a number of difficulties. In the present study, this problem has been resolved by using a plasma etcher, in which a Faraday cage was installed as an auxiliary device in the conventional gas chopping process (or the Bosch process). The conventional gas chopping process has been widely used in microelectromechanical systems (MEMS), providing high-AR Si etch profiles on a nanometer scale (23, 24). However, this etching process is limited in controlling the angle of the etch profile as shown in Fig. 1*A*. In the conventional plasma etching, incident ions are accelerated through the plasma sheath and bombarded within a uniform thickness following the contour of the substrate surface, resulting in a directional etching normal to the surface. Therefore, a simple tilting the slope angle of the substrate would not lead to an angled etching.

To overcome this limitation, a Faraday cage was installed in the conventional plasma etching system, which allowed the control of the angle of ions incident on the substrate surface (25). The cage, a conducting box consisting of a 15-mm-high cylindrical copper sidewall and a stainless-steel grid top plane was fixed to the cathode of the plasma etcher, as shown in Fig. 1*B*. When plasma is ignited, a plasma sheath forms on the cage surface including the grid plane. Ions generated in the plasma accelerate in the sheath and then pass through the opening of the grid plane. Because the inside of the cage is free of electric field, ions maintain their normal direction to the grid plane (26–28). This implies that the direction of ions traveling inside the cage is not affected by the geometry of the substrate placed on the cathode, resulting in an angled etching by tilting the slope of the substrate surface (Fig. 1*B*).

Fig. 1*C* shows scanning electron microscopy (SEM) images of the polySi substrate having slanted nanoholes. The polySi substrate was masked with a 330-nm-thick SiO_2 layer and contained a 100-nm-thick SiO_2 etch-stop layer between the polySi and the Si, as shown in Fig. 1*C*. The size and pitch of the dot patterns are given in Fig. 1*C*. The polySi substrate was etched by using the above plasma etcher modified with the Faraday cage system in the conventional gas chopping process [see supporting information (SI) Fig. S1]. Fig. 1 *D–G* shows the resulting etch profiles. As shown in Fig. 1*D*, etch profiles with angles of 30°, 45°, and 60° were successfully obtained. The angles of the etch profiles were nearly the same as those of the substrate holders, demonstrating that the ion-incident angles could be controlled by using the Faraday cage system.

Fig. 1 *E–G* shows SEM images of the polySi master for the fabrication of nanohairy structures. The polySi etch profiles had an angle of 30° and an aspect ratio of 6.9 (etch depth = 2,840 nm, the hole critical dimension (CD) = 410 nm), as shown in Fig. 1*E*. To enhance the stability and adhesive force of replicated nanohairy structures, several etching techniques were used. One was to use isotropic etching of a polySi substrate before directional etching, which produced an etch profile with a relatively broad top portion, as shown in Fig. 1*E*. Such an etch profile was expected to strengthen the root of nanohairs and, consequently, the stability of nanohairs. The other was to use an etch-stop layer to improve the adhesive force of replicated structures. Because the gas chopping process makes the bottom etch profile round shaped (24, 29) (Fig. 1*D*), the contact fraction of nanohairs replicated from the master was reduced at the time of contact (13). To solve this challenge, an etch-stop layer was imbedded between the polySi and the Si, which produced a relatively flat bottom profile after the etching process (Fig. 1*E*). The tip area could be further increased by using additional etching techniques such as an overetching of the polySi (Fig. 1*F*) and a wet etching of the etch-stop layer (Fig. 1*G*).

Fabrication of Slanted Polymer Nanohairs. After preparing an etched Si master with a specific angle, we fabricated slanted nanohairs by replicating the master with soft UV-curable polyurethane acrylate (PUA), shown in Fig. 2*A*. This PUA material was recently introduced for sub-100-nm patterning. Although PDMS is not well suited for fabricating high-AR, sub-100-nm structures with structural instability (e.g., self-matting problem) (30), the PUA is sufficiently rigid (tunable modulus of 19.8 to ≈320 MPa) and can be made flexible (≈50 μm thickness), to fabricate nanoscale structures with high AR over a large area without a self-matting problem (31, 32). In addition, UV radiation curing enables rapid transformation of a solvent-free liquid resin into a solid polymer at ambient temperature within a few tens of seconds, thereby reducing the process time significantly. In the replication process, it was found that the peeling-off direction of the cured PUA layer is important to prevent a fracture of nanohairs (see Fig. 2*A*).

Fig. 2 *B–F* shows SEM images of inclined PUA nanohairs formed on poly(ethylene terephthalate) (PET) (≈50 μm thickness) film substrate. For replica molding, a polySi substrate having nanoholes with flat bottom was used (see Fig. 1*G*). As shown in the figure, nanohairs slanted with 60° angle with respect to the horizontal plane were uniformly formed over a large area with a high packing density (>130 million hairs per square centimeter). The length of

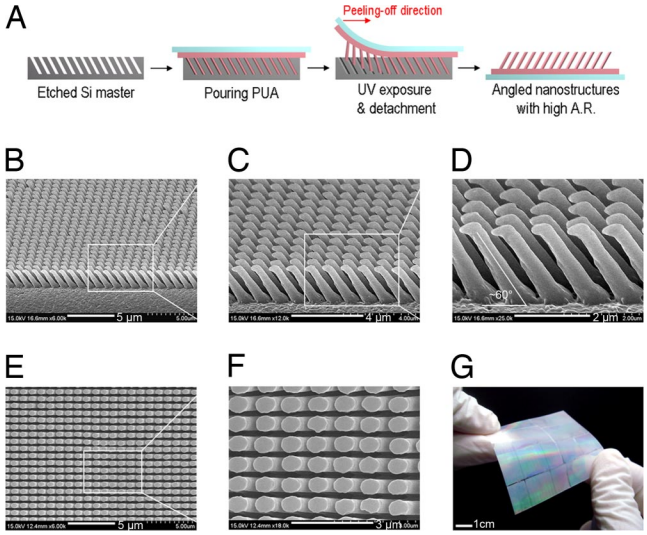

Fig. 2. Fabrication of slanted nanohairs with UV-curable PUA resin. (*A*) Schematic illustration of the fabrication of slanted polymer nanohairs by replica molding with UV-curable PUA resin. (*B*) A titled SEM image of angled, PUA nanohairs. The hairs are 3 μm in height with bottom, neck, and top diameter of 700, 350, and 600 nm, respectively. (*C* and *D*) Magnified, titled images of *B*, showing well-defined PUA nanohairs with bulged flat top and slanted angle of 60° with respect to the horizontal plane. (*E* and *F*) A planar SEM image of the hairs (*E*) and its magnified image (*F*), showing clear spatulae-like flat head. (*G*) A photograph showing large-area fabrication of slanted PUA nanohairs on 50-μm PET film substrate (area = 5 × 5 cm^2).

nanohairs was ≈2.8 μm, and the neck diameter of the structure was 350 nm. In addition, each nanohair has a flat, bulged top that was 600 nm in diameter, similar to that of the gecko's spatula. The bulged tip is advantageous for enhancing the adhesive force as compared with nanohairs with a rounded or a simple flat top. Furthermore, the bottom diameter of the nanohair is 700 nm, leading to high structural stability. A photograph shown in Fig. 2G demonstrates the capability of large-area fabrication with minimum defects (5 × 5 cm^2).

It is worthwhile noting that inclined, high-AR nanoscale structures are difficult to obtain with other methods. Although modified photolithography (9), mechanical machining (33), and soft lithography with a shape-memory thermoplastic (22) have been proposed for fabricating angled polymer structures, the minimum diameters of the structure reported so far are in the range of 10 to ≈1,000 μm, resulting in a reduced adhesive force and directionality (9, 22, 33). Recently, Murphy et al. (13) demonstrated that the adhesion force and directionality can be enhanced by forming flat mushroom-like tips at the end of angled microstructures. This simple approach is useful for fabricating dry adhesive having fairly high adhesion and directionality, but the adhesion force and adaptability to a rough surface would be limited because of a relatively large size of the structures (≈35 μm) Also, traditional MEMS technologies such as LIGA are also difficult to use because of their resolution limit and fabrication complexity. In addition, nanostructures with a directional angle are not easily acquired by growing carbon nanotubes despite their superior structural features such as high AR and extremely small radius (≈10 nm). A patterning area is also potentially limited with carbon nanotubes (≈4 × 4 mm^2) by complicated deposition conditions (photolithography, catalyst deposition, and chemical vapor deposition at high temperature, e.g., ≈750 °C) (20, 21). Compared with these approaches, the current method offers a simple and efficient route to fabricating slanted nanohairs with tailored geometry (angle, radius, height, shape of tip) in a fast and cost-effective manner with minimal fabrication process.

Measurements of Adhesion Strength of Slanted Nanohairs. The macroscopic shear adhesion strength of the gecko-inspired dry adhesive with angled nanohairs was evaluated by a hanging test (see Fig. S2). For these measurements, a flexible dry adhesive (thickness: 50 to ≈60 μm, size: 3 × 1 cm^2) was attached against a smooth Si surface under a preload of 0.3 N/cm^2. During the shear adhesion test, no external normal load was applied. As shown in Fig. 3*A*, the shear adhesion forces were ≈3.2 N/cm^2 and ≈14.5 N/cm^2 for a bare PUA film and vertical nanohairs, respectively. For angled nanohairs, a significant increase in the shear adhesion force was observed (≈26.0 N/cm^2 maximum and ≈21 N/cm^2 on average), which can be attributed to the reduced effective modulus to ≈26.3 kPa (see *SI Text* and Fig. S3) and structural similarity to natural gecko foot hairs (directional angle, size, and spatulae-like head). It appears that the relatively high adhesion of the nonpatterned PUA film despite its high modulus (≈19.8 MPa) originates from the small thickness (50 to ≈60 μm) of the PET film (34). Also, vertical nanohairs are prone to buckling at the time of contact, resulting in a reduced adhesion force compared with that of slanted nanohairs.

It is intriguing that the shear adhesion of angled nanohairs is twice as large as that of gecko foot hairs (≈10 N/cm^2), representing

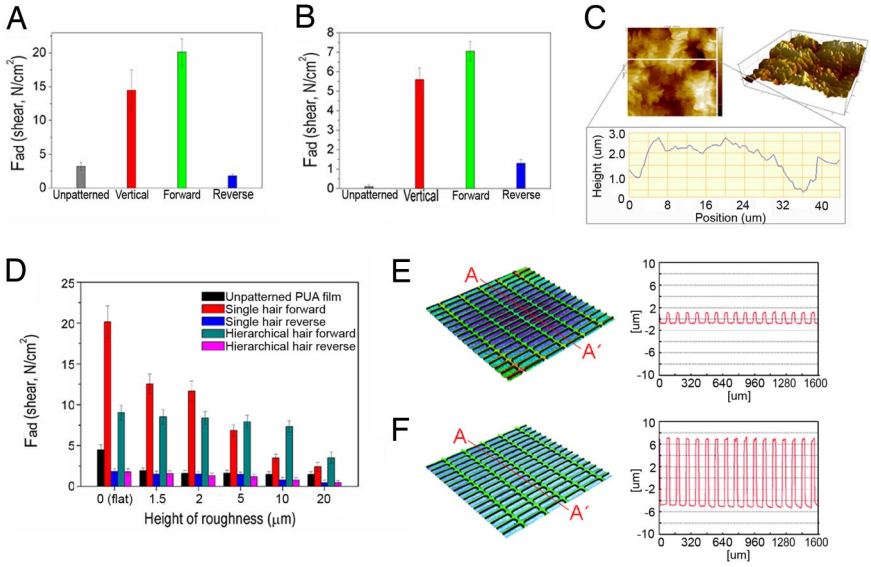

Fig. 3. Adhesion strength of single-scale and multiscale hairs against various substrates. (*A*) Measurement of shear force with an adhesive having nanohairs of 3 × 1 cm^2 in area against a flat Si surface. (*B*) Measurement of shear force with the same adhesive against a rough surface (backside of Si wafer). (*C*) Two- and 3-dimensional AFM micrographs and the corresponding surface profile of the backside of Si wafer used in the roughness adaptation tests of nanohairs. (*D*) Measurement and comparison of shear force with an adhesive patch having single-scale hairs and an adhesive patch having multiscale hierarchical hairs against flat Si and rough Si surfaces with 5 different roughness heights. For rough surfaces, microlattice structures with different heights (1.5, 2, 5, 10, and 20 μm) were used. (*E* and *F*) Three-dimensional micrographs and the corresponding surface profiles of the lattice structures with roughness height of 1.5 (*E*) and 10 (*F*) μm.

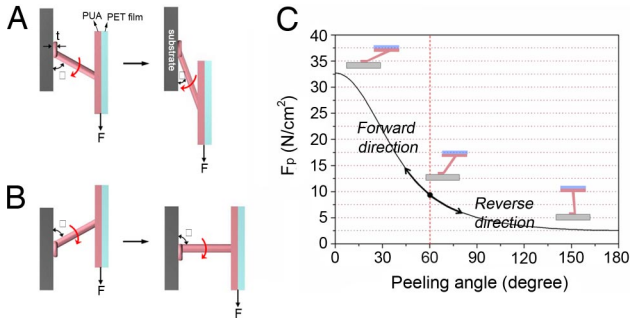

Fig. 4. Thoretical analysis of directional adhesion of the slanted nanohairs. (*A* and *B*) An illustration showing the change of leaning angle of the slanted nanohairs when the dry adhesive is pulled in the forward (*A*) and the reverse (*B*) directions. (C) Critical peel-off forces as a function of peeling angle.

the strongest level among polymer-based artificial dry adhesives reported so far. In parallel, the shear force was greatly reduced to 2.2 N/cm^2 when pulled against the direction of the inclined angle, suggesting that the dry adhesive presented here can be used as a smart, directional adhesive patch with strong attachment (≈26 N/cm^2) and easy detachment (≈2.2 N/cm^2), with the hysteresis close to 10. Moreover, the adhesion force was maintained even after >50 cycles of attachment and detachment (see Fig. S4).

The strong directional adhesion capability mentioned above can be explained by a simple peeling model. According to the Kendall peeling model, the critical peel-off force (F_c) of a nanohair can be estimated with an assumption that the tip of slanted nanohairs forms intimate contact with the substrate as in an elastic tape, yielding (35)

$$F_c = \frac{2\gamma b}{\sqrt{(1-\cos\theta)^2 + \frac{2\gamma}{Et}} + 1 - \cos\theta}, \qquad [1]$$

where γ is the adhesive energy, θ is the peel-off angle, and b, t, and E are the width, thickness, and elastic modulus of the tape, respectively. Thus, the peel-off force can be expressed as a function of peeling angle for given parameters and the total peel-off force per unit area can be expressed by

$$F_p = \frac{2\gamma b D}{\sqrt{(1-\cos\theta)^2 + \frac{2\gamma}{Et}} + 1 - \cos\theta}, \qquad [2]$$

where D represents the hair density. Fig. 4*C* shows the peel-off force per unit area with varying peeling angles. Here, $\gamma = 100$ mJ/m^2, $b =$ 400 nm, $t = 100$ nm, $E = 19.8$ MPa, and $D = 1.3 \times 10^8$/cm^2. As shown in Fig. 4*A*, the slanted angle of nanohairs reduces from its initial leaning angle of 60° and approaches 0° when the dry adhesive is pulled in the forward direction (see Fig. S5). Accordingly, the peel-off force increases gradually with a stronger shear adhesion force. When the adhesive was pulled in the reverse direction (Fig. 4*B*), however, the leaning angle of nanohairs is increased from its initial value of 60° to 180°, and thus the peel-off force is greatly reduced. According to Eq. **2**, the peel-off forces are 30, 5.1, and 2.6 N/cm^2 for 0°, 90°, and 180°, respectively, which agrees with our experimental results (maximum shear adhesion of ≈26 N/cm^2 in the forward direction and ≈2.2 N/cm^2 in the reverse direction).

In addition to shear adhesion tests to a flat surface, the adhesion capability against a rough surface was also measured by using the back side of an Si wafer. As shown in Fig. 3*C*, the back side of the Si wafer is rough with randomly distributed peaks and valleys (roughness of root mean square ≈674 nm) with its maximum height >3 μm. As a result, even soft materials (e.g., PDMS), which easily attach to flat surfaces, hardly attach to this surface. As shown in Fig. 3*B*, the shear force of a flat, nonpatterned PUA film against the surface was nearly zero. The dry adhesive having angled high-AR nanohairs showed a fairly high adhesion force (≈7 N/cm^2), demonstrating the smart adhesion capability of the current gecko-inspired tape to surfaces of varying roughness. It is noted that the adhesive force against a rough surface is much smaller than that against a flat surface (≈21 N/cm^2). This is for several reasons. The first is that the tip size of pillars (≈600 nm) is not small enough to safely penetrate in the valleys (roughness = 674 nm) and then conformably touch the bottom surface (36). The second is that the limited height of nanohairs (≈2.8 μm) diminishes the contact fraction of hairs at the time of contact for a given preload. To overcome this problem, the height of nanohairs needs to be increased, but it is restricted by a critical value that is involved in lateral collapse of hairy structures. For example, the maximum height (h_{max}) attainable for given elastic modulus, size and surface energy of nanohairs is given by (37)

$$h_{max} = \left(\frac{\pi^4 ER}{2^{11}\gamma_s(1-\nu^2)}\right)^{1/12} \times \left(\frac{12ER^3(W/2)^2}{\gamma_s}\right)^{1/4}, \qquad [3]$$

where R is the radius of hair, r_s is the surface energy, W is the distance of 2 neighboring hairs, E is the elastic modulus of hair, and ν is the Poisson's ratio. According to Eq. **3**, the maximum height of slated nanohairs is in the range of 2 to ≈3 μm ($r_s = 40$ mJ/m^2 and $\nu = 0.5$), corresponding to the height of slanted hairs presented here (≈2.8 μm).

Fabrication and Measurements of Adhesion Strength of Micro-/Nanoscale Hierarchical Hairs. Recent theoretical studies have revealed that the hierarchy of structures can give rise to increased adhesion strength against a rough surface either by reducing structural stiffness or by enhancing structural height without instability (14, 15). Based on these observations, we fabricated monolithic, micro-/nanoscale combined hierarchical polymer hairs by a 2-step UV-assisted capillary molding technique. Fig. 5*A* shows a schematic diagram of the fabrication procedure (38). For fabricating a microscopic setae-like structure (first step), a micropatterned PDMS mold (see Fig. S6*A*) was placed onto a spin-coated, UV-curable PUA resin on a thin PET substrate, followed by partial curing by exposure to UV light for 50 s (λ = 250–400 nm, dose = 100 mJ/cm^2). Fabrication of spatulae-like, slanted nanohairs on the preformed microstructure was subsequently carried out by applying a nanoscale PUA mold. The PUA mold was self-replicated from the angled PUA nanohairs (see Fig. S6*B*), which was placed on top of the as-prepared microstructure with a low pressure (10^3 Pa), followed by an additional UV exposure for 10 s. A key finding is that a partially cured microstructure can be further molded by sequential application of a nanopatterned mold with the aid of inhibitory effects of trapped or permeated oxygen within cavities at the mold/polymer interface, resulting in a monolithic hierarchical structure.

Fig. 5*B* shows SEM images of multiscale hierarchical PUA hairs on a PET (≈50 μm thickness) film substrate. As shown in the figure, well-defined angled, high-AR nanohairs with a protruding flat head (exactly the same with those shown in Fig. 2) were uniformly formed on top of 5-μm hairs (spacing of 5 μm, height of 25 μm) over a large area without collapse of the underlying microstructures. The size of the microhairs (diameter of 5 μm and height of 25 μm) was selected by considering the actual size of gecko's setae (diameter of 5 μm and height of 100 μm) (see Fig. S7). The height of the microstructures, however, was limited to ≈40 μm (see Eq. **3**) because of structural instability caused by a relatively low elastic modulus of soft PUA (19.8 MPa). One notable feature is that there is no interface between micro- and nanohairs, which is one of advantages of the 2-step UV-assisted molding method presented here. These monolithic, multiscale structures are especially useful for an artificial dry adhesive because it can enhance structural

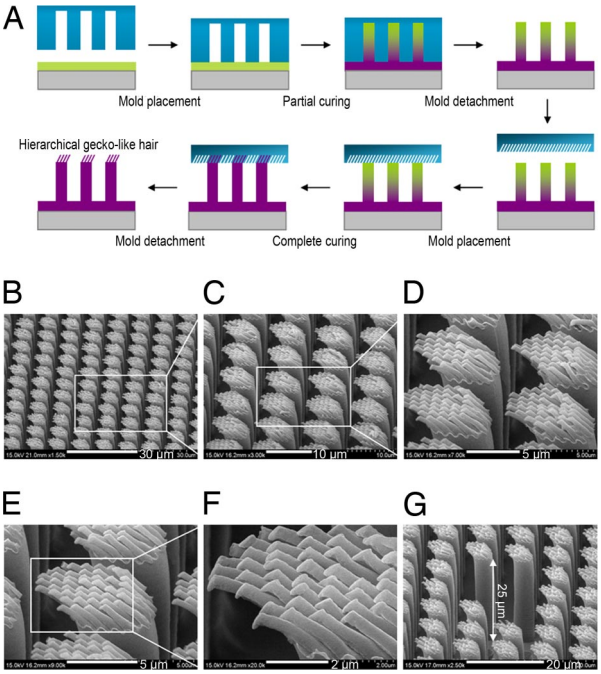

Fig. 5. Fabrication of hierarchical hairs with UV-curable PUA resin. (*A*) A schematic illustration for the fabrication of dual-scale hierarchical gecko-like hairs by 2-step UV-assisted capillary force lithography. (*B*) A titled SEM image of 2-level hierarchical PUA hairs formed over a large area. (*C*–*G*) Magnified, titled images of *B*, showing well-defined high-AR and angled nanohairs with bulged flat top formed on 5-μm pillars (5-μm spacing, 25-μm height).

integrity and mechanical strength without an interface failure under an external load.

To elaborate on the adhesion capability of the multiscale hierarchical PUA hairs, we measured shear adhesion against surfaces with different roughness. Fig. 3*D* shows the results by using simple nanohairs and micro-/nanoscale hierarchical hairs against walls with different magnitude of roughness (0, 1.5, 2, 5, 10, and 20 μm; see Fig. 3 *E* and *F*). As shown in the figure, the adhesive force of simple nanohairs against a flat surface was larger ($\approx$21 N/cm^2) than that of hierarchical hairs ($\approx$9 N/cm^2). One of the reasons is that unlike tree-like, hierarchical gecko foot hairs, the density of nanohairs formed on microhairs is lower than that of simple nanohairs. The adhesive force of simple nanohairs, however, rapidly decreased with increasing the magnitude of the surface roughness, whereas that of hierarchical hairs maintained or slightly decreased with increasing roughness up to 10 μm. This is presumably because the actual height of hierarchical hairs is greatly increased ($\approx$25 μm), thereby penetrating into the valleys of a rough surface and forming a conformal contact. When the roughness was increased to 20 μm, the adhesion strength of hierarchical hairs was significantly reduced to 3.51 N/cm^2, suggesting that there is a maximum deformation allowable for the hierarchical hairs (14). For both single-scale and multiscale hairs, the directional adhesion property was almost the same (strong attachment and weak detachment).

Application of Nontransferring Dry Adhesive with Slanted Nanohairs. To seek practical applications of the dry adhesive reported here, we developed a clean transport system by exploiting directional adhesion characteristic. In the liquid crystal display (LCD) industry, a very thin glass substrate (<1 mm thickness) should be accurately transported without surface contamination in vacuum during the process of LCD panel assembly. In particular, suction or mechanical holding is difficult to implement in a vacuum. Currently, an electrostatic chuck (ESC) is used, which is too costly (approximately $350,000, just for ESC holding chuck of the LCD alignment system)

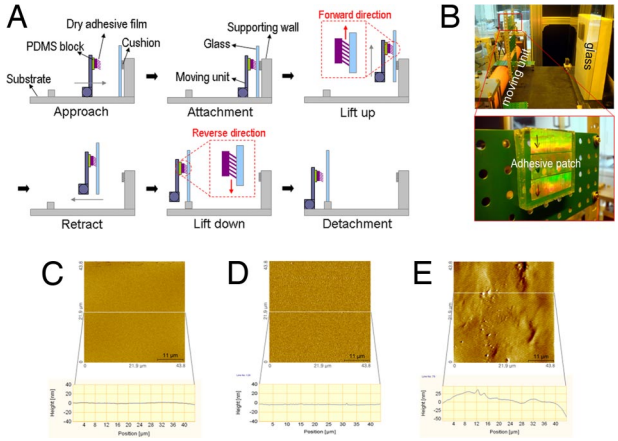

Fig. 6. Demonstration of the clean transportation system with a dry adhesive patch. (*A*) A schematic illustration of the LCD transport process with a gecko-inspired dry adhesive. When the adhesive patch is pulled along the forward direction, the glass panel can be firmly lifted, whereas it can be easily detached by pulling the patch along the opposite direction. (*B*) A photograph of the LCD glass transport system (*Upper*) and a magnified photograph showing the dry-adhesive patch integrated with the system (*Lower*). (*C* and *D*) Two-dimensional AFM micrographs and corresponding cross-sectional profiles of the glass surface before (*C*) and after (*D*) attachment of the dry adhesive. (*E*) A 2-dimensional AFM micrograph and the corresponding surface profile of the glass surface after attachment of a pressure-sensitive tape. The surface was fouled with sticky molecules transferred from the tape.

and might lead to surface contamination or damage because of the high electric field applied to the substrate. In this regard, a gecko-inspired dry adhesive has the potential to replace the current ESC holding system because it enables directional adhesion without fouling by sticky materials after many cycles of attachment and detachment. To demonstrate the transport of an LCD glass panel, we devised a simple experimental setup as shown in Fig. 6 *A* and *B*. The LCD glass used in this experiment was 0.9 mm in thickness and 47.5 $\times$ 37.5 cm^2 in size. Before attachment to the glass panel, a dry adhesive (3 $\times$ 3 cm^2) was attached to the moving unit, which then approached the glass, forming a conformal contact with the aid of a thin PDMS block and a sponge-like cushion that had been sealed onto the back side of the dry adhesive and the glass panel, respectively. After forming firm attachment of the dry-adhesive with nanohairs drooping downward, the moving unit started to move upward, lifting the glass panel by the shear adhesion of the dry adhesive. After arriving at a target location, the moving unit started to move downward, releasing the panel from the adhesive with the aid of a support box that had been placed on a releasing position (see Movie S1). The support box acted as a separator from the adhesive when pulling the dry adhesive along the opposite direction.

To verify that no contamination of trace or dirt on the glass panel occurs during the transport, the surface morphology was carefully examined by atomic-force microscopy (AFM) measurements before and after attachment of the adhesive. The results demonstrated that there was essentially no difference between contacting surfaces, such that the glass surface remained clean even after use of an adhesive patch (Fig. 6 *C* and *D*). In contrast, the surface was contaminated immediately after use of a pressure sensitive tape, suggesting that materials can be easily transported to the attaching surface (Fig. 6*E*).

Conclusions

We have presented an approach for the fabrication of inclined, polymer nanohairs for their use as a nontransferring gecko-like dry adhesive. For the fabrication, we have used an angled etching technique equipped with a Faraday cage to produce slanted nanoholes, followed by replica molding with an UV-curable resin. By

controlling etching conditions, various nanohairs were faithfully replicated with tailored geometry (angle, radius, height, shape of tip, and hierarchy). The angled PUA nanohairs with a bulged flat top showed excellent directional adhesion, exhibiting strong shear attachment (≈26 N/cm^2) in the forward direction (pulled in the angled direction of hairs) and easy detachment (≈2.2 N/cm^2) in the reverse direction (pulled against the angled direction of hairs). In addition to single-scale nanohairs, monolithic, hierarchical hairs were also fabricated by a 2-step UV-assisted molding technique. The resulting hierarchical hairs showed fairly high adhesion capability even on a rough surface (roughness <20 μm) without structural instability, whereas the simple nanohairs showed reduced adhesion with increasing the surface roughness to ≈5 μm. A unique application of the adhesive patch with angled nanohairs was demonstrated by transporting a large-area glass panel without surface contamination based on the directional adhesion characteristic, revealing that the truly biomimetic dry adhesive presented here could be an alternative for a clean transport/holding system for the LCD industry and other biomimetic applications.

Materials and Methods

Preparation of a polySi Wafer. The polySi wafer was prepared as follows: First, a 100-nm-thick SiO_2 film was thermally grown on a *p*-type and 6-in Si (100) wafer. Then, a 2,700-nm-thick polySi layer was deposited by a low-pressure chemical vapor deposition (LPCVD) process. Finally, a 330-nm-thick SiO_2 film was deposited by plasma-enhanced chemical vapor deposition (PECVD) by using tetraethoxysilane (TEOS) as a SiO_2 source and was patterned by using conventional photolithography and etching techniques.

Angled Etching of polySi Substrates. The polySi substrate was attached on the substrate holder inside the Faraday cage by using a silver paste that provided a good thermal and electrical contact between the substrate and the holder. The slope angles of the substrate holders were 30°, 45°, and 60°. The substrate was subjected to isotropic etching in SF_6/Ar plasma. Subsequently, the substrate was etched by using the gas chopping process, which consisted of alternating etching (80 s) and deposition steps (8 s). In the case of etch profiles shown in Fig. 1*F*, 16 cycles of the gas chopping process were repeated. Details can be found in *SI Text*.

Fabrication of Angled, High-Aspect-Ratio Nanohairs. The PUA was composed of a functionalized prepolymer with acrylate groups for cross-linking, a monomeric modulator, a photoinitiator and a radiation-curable releasing agent for surface activity. The liquid mixture was drop-dispensed onto a polysilicon master with slanted holes and a PET film with 50-μm thickness was gently placed on the liquid mixture, followed by UV (λ = 250 to ≈400 nm) exposure for a few tens of seconds. After the UV curing, the mold was peeled off from the master, leaving behind angled, high-AR PUA nanohairs.

Fabrication of Micro-/Nanoscale Hierarchical Hairs. Our fabrication method is based on a sequential application of capillary molding for generating micro-/nanoscale hierarchical structures. For fabricating polymer microhairs, a PDMS mold having micropatterns was placed onto the spin-coated, UV-curable PUA resin on the flexible PET substrate (50 μm thickness). Then the PUA resin was partially cured by UV exposure for 50 s (λ = 250–400 nm, dose = 100 mJ/cm^2). After fabricating a partially cured microstructure, the PUA mold with angled nanopatterns was placed on the preformed microhairy structures under a slight pressure (≈10 g/cm^2), followed by additional UV exposure for 10 s. The resulting hierarchical hairs are very similar to real gecko foot hairs as shown in Fig. S7. Details can be found in *SI Text*.

Shear Adhesion Tests. The macroscopic shear adhesion strength of the angled nanohairs was evaluated by a hanging test. A flexible adhesive patch (thickness: 50 to ≈60 μm, area = 1 × 3 cm^2) was attached onto the surface under a preload of ≈0.3 N/cm^2, and then the hanging weight was increased until an adhesion failure occurred. To investigate the directional adhesion properties of the adhesive, weight was applied along (forward) and against (reverse) the angled directions of the slanted hairs. For comparison, the shear adhesion strength of the nonpatterned PUA film was also evaluated by attaching the film (thickness $<$60 μm, area = 1 × 3 cm^2) onto the surface under a preload of ≈0.3 N/cm^2. The nonpatterned PUA film was obtained by spincoating a PUA liquid on a thin PET film (50-μm thickness) and subsequent exposure to UV for a few tens of seconds. The actual contact area of nonpatterned surface is ≈2.7 times higher than that of structured surface.

ACKNOWLEDGMENTS. We thank Dr. Khademhosseini for his enthusiastic discussion and comments. This work was supported by the Korea Science and Engineering Foundation through Nano R&D Program Grant 2007-02605, the Micro Thermal System Research Center of Seoul National University, National Research Laboratory Program Grant M10104000095-01J0000-04210, and the Center for Ultramicrochemical Process Systems. This work was also supported in part by King Abdullah University of Science and Technology Program KUK-F1-037-02 and a Korea Research Foundation Grant funded by the Korean Government Ministry of Education and Human Resource Development Grant KRF-J03000.

1. Packham DE (2005) *Handbook of Adhesion* (Wiley, Hoboken, NJ).
2. Lee H, Lee BP, Messersmith PB (2007) A reversible wet/dry adhesive inspired by mussels and geckos. *Nature* 448:338–U334.
3. Autumn K, et al. (2000) Adhesive force of a single gecko foot-hair. *Nature* 405:681–685.
4. Autumn K, et al. (2002) Evidence for van der Waals adhesion in gecko setae. *Proc Natl Acad Sci USA* 99:12252–12256.
5. Greiner C, del Campo A, Arzt E (2007) Adhesion of bioinspired micropatterned surfaces: Effects of pillar radius, aspect ratio, and preload. *Langmuir* 23:3495–3502.
6. Spolenak R, Gorb S, Arzt E (2005) Adhesion design maps for bio-inspired attachment systems. *Acta Biomaterialia* 1:5–13.
7. del Campo A, Greiner C, Alvarez I, Arzt E (2007) Patterned surfaces with pillars with controlled 3D tip geometry mimicking bioattachment devices. *Adv Mater* 19:1973–1977.
8. Mahdavi A, et al. (2008) A biodegradable and biocompatible gecko-inspired tissue adhesive. *Proc Natl Acad Sci USA* 105:2307–2312.
9. Aksak B, Murphy MP, Sitti M (2007) Adhesion of biologically inspired vertical and angled polymer microfiber arrays. *Langmuir* 23:3322–3332.
10. Autumn K, Majidi C, Groff RE, Dittmore A, Fearing R (2006) Effective elastic modulus of isolated gecko setal arrays *J Exp Biol* 209:3558–3568.
11. Arzt E, Gorb S, Spolenak R (2003) From micro to nano contacts in biological attachment devices. *Proc Natl Acad Sci USA* 100:10603–10606.
12. Autumn K, Dittmore A, Santos D, Spenko M, Cutkosky M (2006) Frictional adhesion: A new angle on gecko attachment *J Exp Biol* 209:3569–3579.
13. Michael P (2009) Murphy BAMS gecko-inspired directional and controllable adhesion. *Small* 5:170–175.
14. Bhushan B, Peressadko AG, Kim TW (2006) Adhesion analysis of two-level hierarchical morphology in natural attachment systems for 'smart adhesion'. *J Adhes Sci Technol* 20:1475–1491.
15. Yao H, Gao H (2006) Mechanics of robust and releasable adhesion in biology: Bottom-up designed hierarchical structures of gecko. *J Mech Phys Solids* 54:1120–1146.
16. Michael T (2008) Northen CGEAKLT a gecko-inspired reversible adhesive. *Adv Mater* 20:3905–3909.
17. Geim AK, et al. (2003) Microfabricated adhesive mimicking gecko foot-hair. *Nat Mater* 2:461–463.
18. Jeong HE, Lee SH, Kim P, Suh KY (2006) Stretched polymer nanohairs by nanodrawing. *Nano Lett* 6:1508–1513.
19. Majidi C, et al. (2006) High friction from a stiff polymer using microfiber arrays. *Phys Rev Lett* 97:076103.
20. Ge L, Sethi S, Ci L, Ajayan PM, Dhinojwala A (2007) Carbon nanotube-based synthetic gecko tapes. *Proc Natl Acad Sci USA* 104:10792–10795.
21. Qu LT, Dai LM, Stone M, Xia ZH, Wang ZL (2008) Carbon nanotube arrays with strong shear binding-on and easy normal lifting-off. *Science* 322:238–242.
22. Reddy S, Arzt E, del Campo A (2007) Bioinspired surfaces with switchable adhesion. *Adv Mater* 19:3833–3837.
23. Rangelow IW (2003) Critical tasks in high aspect ratio silicon dry etching for microelectromechanical systems. *J Vac Sci Technol A* 21:1550–1562.
24. Wang X, Zeng W, Lu G, Russo OL, Eisenbraun E (2007) High aspect ratio Bosch etching of sub-0.25 μm trenches for hyperintegration applications. *J Vac Sci Technol B* 25:1376–1381.
25. Cho BO, Hwang SW, Ryu JH, Kim IW, Moon SH (1999) Fabrication method for surface gratings using a Faraday cage in a conventional plasma etching apparatus. *Electrochem Solid State Lett* 2:129–130.
26. Ryu JH, Cho BO, Hwang SW, Moon SH, Kim CK (2003) Trajectories of ions inside a Faraday cage located in a high density plasma etcher. *Kor J Chem Eng* 20:407–413.
27. Lee JK, Lee GR, Min JH, Moon SH (2006) Angular distribution of particles sputtered from Si bottom in a CHF3 plasma. *J Vac Sci Technol A* 24:1807–1811.
28. Min JH, Lee JK, Moon SH (2005) Deep etching of silicon with smooth sidewalls by an improved gas-chopping process using a Faraday cage and a high bias voltage. *J Vac Sci Technol B* 23:1405–1411.
29. Craigie CJD, et al. (2002) Polymer thickness effects on Bosch etch profiles. *J Vac Sci Technol B* 20:2229–2232.
30. Hui CY, Jagota A, Lin YY, Kramer EJ (2002) Constraints on microcontact printing imposed by stamp deformation. *Langmuir* 18:1394–1407.
31. Suh D, Choi SJ, Lee HH (2005) Rigiflex lithography for nanostructure transfer. *Adv Mater* 17:1554–1560.
32. Choi SJ, Yoo PJ, Baek SJ, Kim TW, Lee HH (2004) An ultraviolet-curable mold for sub-100-nm lithography. *J Am Chem Soc* 126:7744–7745.
33. Santos D, Spenko M, Parness A, Kim S, Cutkosky M (2007) Directional adhesion for climbing: Theoretical and practical considerations. *J Adhes Sci Technol* 21:1317–1341.
34. Kim S, Sitti M, Hui CY, Long R, Jagota (2007) Effect of backing layer thickness on adhesion of single-level elastomer fiber arrays. *Appl Phys Lett* 91:161905.
35. Kendall K (1975) Thin-film peeling-the elastic term. *J Phys D* 8:1449.
36. Pugno NM, Lepore E (2008) Observation of optimal gecko's adhesion on nanorough surfaces. *Biosystems* 94:218–222.
37. Glassmaker NJ, Jagota A, Hui CY, Kim J (2004) Design of biomimetic fibrillar interfaces: 1. Making contact. *J R Soc Interface* 1:23–33.
38. Jeong HE, Kwak R, Kim JK, Suh KY (2008) Generation and self-replication of monolithic, dual-scale polymer structures by two-step capillary-force lithography. *Small* 4:1913–1918.